ACS APPLIED MATERIALS & INTERFACES

Research Article

www.acsami.org

High-Performance Polymer Solar Cells with Solution-Processed and Environmentally Friendly CuO_x Anode Buffer Layer

Qi Xu,[†] Fuzhi Wang,[†] Zhan'ao Tan,*[,†] Liangjie Li,[†] Shusheng Li,[†] Xuliang Hou,[†] Gang Sun,[†] Xiaohe Tu,[†] Jianhui Hou,[‡] and Yongfang Li*[,‡]

[†]State Key Laboratory of Alternate Electrical Power System with Renewable Energy Sources, Beijing Key Laboratory of Energy Security and Clean Utilization, North China Electric Power University, Beijing 102206, China

[‡]Beijing National Laboratory for Molecular Sciences, Institute of Chemistry, Chinese Academy of Sciences, Beijing 100190, China

Supporting Information

ABSTRACT: Highly efficient polymer solar cells (PSCs) are demonstrated by introducing environmentally friendly CuO_x as hole extraction anode buffer layer. The CuO_x buffer layer is prepared simply via spin-coating 1,2-dichlorobenzene solution of Copper acetylacetonate on the ITO substrate and thermal transformation (at 80 °C) in air. Remarkable improvements in the open-circuit voltage (V_{oc}) and short-circuit current density (J_{sc}) of the PSCs could be achieved upon the introduction of CuO_x buffer layer. The study about the effect of CuO_x interfacial layer on the device resistances demonstrates that insertion of CuO_x layer can decrease the whole resistance of the PSCs. For the devices based on P3HT:PCBM, the power conversion efficiency (PCE) was increased from 2.8% (the reference device without buffer layer) to 4.1% via introduction of CuO_x hole extraction layer. The PCE of the PSC was further increased to 6.72% when ICBA used as an alternative acceptor to PCBM. The much higher PCE of 7.14% can be achieved by adopting PBDTTT-C, a low band gap conjugated polymer, as donor material. The results demonstrate that CuO_x has great potential as a hole extraction material for highly efficient PSCs.

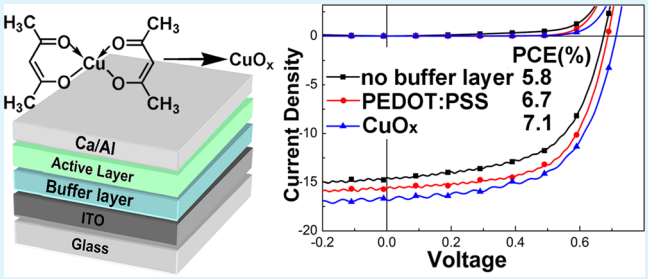

KEYWORDS: *polymer solar cells, anode buffer layer, copper oxides, solution processing*

1. INTRODUCTION

Polymer solar cells (PSCs) have attracted considerable interest because of their advantages of low cost, ease of processing and low environmental pollution.[1−5] Bulk heterojunction structure, in which conjugated polymer donors/fullerene acceptors blended film sandwiched between the anode and cathode, is the most commonly used architecture in PSCs. Over the past few years, great improvements have been gained for the power conversion efficiency (PCE) of PSCs,[6−9] such as the achievements of certified PCE of 9.2%[9] for single-junction and 10.6%[10] for tandem solar cells. Although the PCE is rapidly approaching to the threshold of 10% for commercial application of the PSCs,[9,10] the poor stability of the devices is still the bottleneck for large-scale commercialization. Beside thermal and photo stable photoactive materials, interfacial material is another critical factor for stability improvement. In conventional PSCs, poly(3,4-ethylenedioxythiophene): poly(styrenesulfonate) (PEDOT:PSS) is usually used to modify the anode interface to improve the hole collection ability. Although the commercial available PEDOT:PSS shows good processability, transparency, and electrical conductivity when serving as hole-transport layer,[11,12] it also has a negative effect on the device stability,[13,14] which causes chemistry instability[13−15] and morphology change[13−16] because of its acidity and hygroscopic property.

Metal oxides, such as MoO_3, V_2O_5, WO_3, and NiO, are demonstrated to be promising substitutes for PEDOT:PSS as hole collection materials. However, most of these materials in earlier studies were mainly deposited by vacuum based deposition techniques, which is incompatible with solution processing technique in PSCs. Very recently, solution-processable metal oxides have drawn great attention as hole collection layer for high-performance PSCs.[17−23] However, toxicity of these materials (such as V_2O_5 and NiO) and shortage in the supply of the key metal materials (such as tungsten), are serious problems for practical application. Therefore, there is an urgent demand to develop nontoxic and solution-processable electrode modification layer with naturally earth-abundant elements for highly efficient PSCs.

CuO and Cu_2O, two stable phases of Cu−O system, are well-known p-type semiconductors with high concentration of Cu vacancies and stable defects under both O-rich and Cu-rich conditions.[24−26] The advantages of earth-abundant source, low cost, nontoxicity, and simplicity of preparation make them promising candidates for photovoltaic applications.[27−32] The

Received: July 10, 2013
Accepted: October 4, 2013
Published: October 4, 2013

 © 2013 American Chemical Society

CuO_x can be applied to modulate the barrier between the organic layer and the anode, because the Cu_2O and CuO can form an ohmic contact with ITO.[33] CuO_x is mainly used as photoactive materials in inorganic solar cells, and there are rare reports in the literature using solution-prepared CuO_x for anode modification in PSCs.[32]

In this work, we prepared the CuO_x buffer layer through a low temperature and inexpensive method of spin-coating a copper acetylacetonate ($Cu(acac)_2$) 1,2-dichlorobenzene solution onto ITO and annealing at 80 °C. The solution-processed CuO_x layer shows excellent hole extraction property and high transparency in the visible range. The device with CuO_x anode buffer layer demonstrated improved photovoltaic performance compared with the reference device with PEDOT:PSS anode buffer layer. By using CuO_x as anode buffer layer, P3HT:PCBM-based and P3HT:ICBA-based PSCs reached respective PCE of 4.10% and 6.72%. An even higher PCE up to 7.14% could be achieved by adopting a low band gap conjugated polymer poly(4,8-bis-alkyloxybenzo(1,2-b:4,5-b′)dithiophene-2,6-diyl-alt-(alkyl thieno(3,4-b) thiophene-2-carboxylate)-2,6-diyl) (PBDTTT-C), as donor material.

2. EXPERIMENTAL DETAILS

Nine types of device structures are constructed to study the effect of the CuO_x interlayer on the PSCs performance and the compatibility of CuO_x buffer layer with different materials. The most commonly used P3HT and classical D−A low bandgap copolymer PBDTTT-C[34] were chosen as electron donor, and PCBM, $PC_{70}BM$ and ICBA[35] as electron acceptor, respectively. The molecular structures of the materials involved are given in Figure 1. On the basis of the

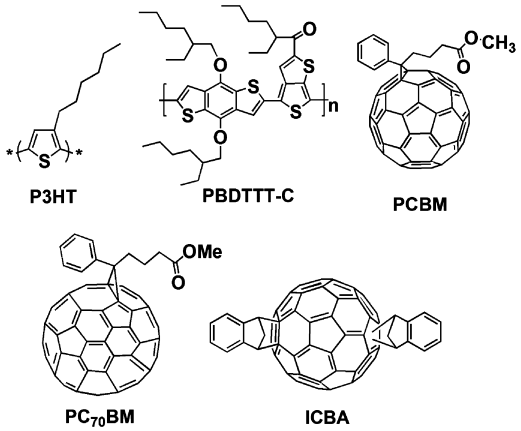

Figure 1. Molecular structures of P3HT, PBDTTT-C, PCBM, $PC_{70}BM$, and ICBA.

aforementioned materials, the device structures are as follows: (A) ITO/P3HT:PCBM (230 nm)/Ca/Al, (B) ITO/PEDOT:PSS/P3HT:PCBM (230 nm)/Ca/Al, (C) ITO/CuO_x/P3HT:PCBM (230 nm) /Ca/Al, (D) ITO/P3HT:ICBA (230 nm)/Ca/Al, (E) ITO/PEDOT:PSS/P3HT:ICBA (230 nm)/Ca/Al, (F) ITO/CuO_x/P3HT:ICBA (230 nm)/Ca/Al, (G) ITO/PBDTTT-C:$PC_{70}BM$ (80 nm)/Ca/Al, (H) ITO/PEDOT:PSS/PBDTTT-C:$PC_{70}BM$ (80 nm)/Ca/Al, and (I) ITO/CuO_x/PBDTTT-C:$PC_{70}BM$ (80 nm)/Ca/Al. Devices A, D and G are reference devices without anode buffer layer, and devices B, E, and H are reference devices with PEDOT:PSS as the anode buffer layer.

The PSCs were fabricated on precleaned and ultraviolet-ozone treated ITO substrate (10 Ω/□). For reference devices B, E and H, poly(3,4-ethylenedioxythiophene):poly(styrenesulfonate) (PEDOT:PSS) (Clevious P VP AI 4083) was spin-coated on the ITO substrate to form a 30 nm film and baked at 150 °C for 10 min. For devices C, F, and I, CuO_x film was fabricated by spin-coating (4000 rpm, 30 s) a 1 mg/mL $Cu(acac)_2$ 1,2-dichlorobenzene solution on the pretreated ITO substrate, and then annealing in air at 80 °C for 20 min. The thickness of the CuO_x layer was ca. 10 nm, determined from its absorbance at 300 nm. After slowly cooled to room temperature, the CuO_x film was washed by spin-coating methanol on top of the CuO_x surface, and followed by 15 min UV-ozone treatment. The active layers were prepared according to the procedures described in our previously published articles[4a,4c,4f]. Finally, a 10 nm Ca and a 100 nm Al were deposited through vapor deposition.

The measurement of the device was carried out under a nitrogen atmosphere in a glovebox. The current density−voltage (J−V) characteristics were measured using a Keithley 236 Source Measure Unit under simulated AM1.5G spectrum with a xenon-lamp-based solar simulator (from Newport Co., LTD), and the light intensity was 100 mW cm^{-2}.

X-ray photoelectron spectroscopy (XPS) was carried out by an ESCA Lab220i-XL electron spectrometer (base pressure of about 3×10^{-9} mbar) from VG Scientific using 300W Al Kα radiation. For cyclic voltammetry (CV) test, a Pt plate coated with a thin CuO_x film, a Pt wire and an Ag/Ag^+ electrode were used as working electrode, counter electrode and reference electrode respectively. Atomic force microscope (AFM) images were achieved on a VEECO DICP-II in tapping mode. The transmittance measurements of the ITO and ITO/CuO_x were conducted on a Hitachi U-3010 UV−vis spectrophotometer. The AC impedance spectroscopy and the electrochemical CV were measured with a CHI650D Electrochemical Workstation. For impedance measurement, an ac signal of 10 mV was applied in the frequency range of 1 Hz−10 MHz.

3. RESULTS AND DISCUSSION

XPS measurement was performed to study the chemical component of the buffer layer before and after annealing, as shown in Figure 2. The XPS spectra are corrected by the C 1s peak of 284.8 eV. The characteristic peaks of the elements Cu, O, and C are shown in the survey scan (Figure 2a). Figure 2b shows the main and the satellite peaks of Cu $2p_{1/2}$ and Cu $2p_{3/2}$ of the samples without or after annealing at 80 °C for 20 min. For $Cu(acac)_2$, the sample without annealing, Cu 2p spectrum consists of two sets of peaks, and each of them shows triple-peak feature. The most intense Cu $2p_{3/2}$ peak appeared at 934.2 eV corresponds to a well-screened final state ($2p^53d^{10}\underline{L}_1$), and the two shakeup peaks (about 939.0−944.4 eV) corresponds to the bonding and antibonding states of the other well-screened ($2p^53d^{10}\underline{L}_2$) and poorly screened states ($2p^53d^9$).[36] Representative Cu 2p spectra for the sample, which is treated by first annealing at 80 °C for 20 min and then UV-ozone treating for 15 min (see Scheme 1), are also displayed in Figure 2b. The intense shakeup satellites centered on the high-binding-energy side of the main peak are evident and diagnostic of a d^9 configuration in the ground state, corresponding to Cu(II) systems.[37−40] The peak positions and relative intensities of the satellites indicate the presence of CuO at the surface. The peaks for the Cu $2p_{3/2}$ spectrum are used to analyze surface chemical component. As shown in Figure 2c, the broad Cu $2p_{3/2}$ peak is deconvoluted into two peaks, peak 1 and peak 2, which are related to Cu_2O (peak 1) and CuO (peak 2), respectively.[38] Cu^+ has a single peak at 932.7 eV with a full width at half-maximum of 1.9 eV, whereas Cu^{2+} has one main peak at 934.9 eV with a fwhm of 2.8 eV and shakeup satellites at higher binding energies. Cu^{2+}/Cu^+ ratio obtained from the deconvolution of the Cu $2p_{3/2}$ peak is about 2.2:1.

The transmittance spectra of ITO/CuO_x and ITO/PEDOT:PSS are shown in Figure S1 in the Supporting Information. The ITO/CuO_x substrate shows similar transmittance from 300 to 900 nm with ITO/PEDOT:PSS

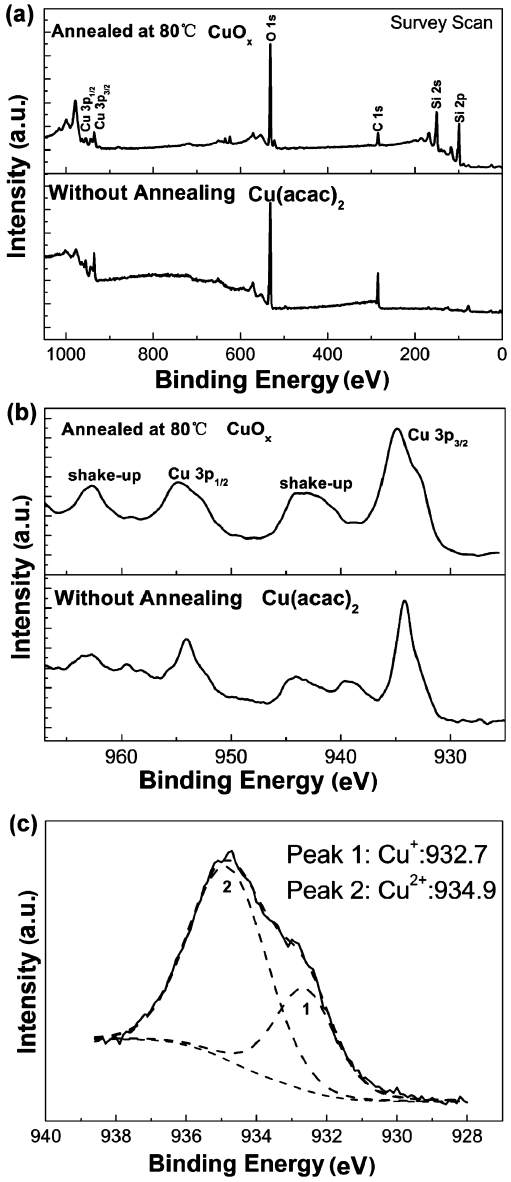

Figure 2. XPS of CuO_x and $Cu(acac)_2$ films on silicon substrate. (a) Survey scan, (b) Cu 2p core level spectra, and (c) typical deconvolution of Cu $2p_{3/2}$ main peak of CuO_x.

Scheme 1. Transformation of Copper Acetylacetonate into Copper Oxide by Thermal Annealing at 80 °C for 20 min in Air

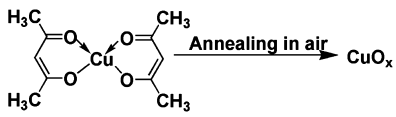

substrate. The ITO/PEDOT:PSS substrate exhibits higher transmittance than bare ITO, which might be attributed to the fact that a smoother surface with root-mean-square (rms) roughness of 1.7 nm (Figure 3b) could be achieved upon modification of PEDOT:PSS.[41]

The tapping mode AFM images of bare ITO and ITO/CuO_x are shown in images a and c in Figure 3. The rms roughness of the ITO/CuO_x substrate is only 1.9 nm, which is comparable to that of PEDOT:PSS-modified ITO substrate, and much smaller than that of bare ITO (3.2 nm). In other words, a smoother surface could be achieved through utilization of CuO_x interlayer. The smoother interface could enable the formation of a better contact between the CuO_x layer and the photoactive layer, hence improve the hole collection efficiency. Apart from that, the decreased roughness is also conducive to the formation of high-quality upper photoactive layer.[42] The height image of the surface of the blend layers are illustrated in Figure 3d–i. Upon insertion of CuO_x interlayer, the rms roughness of the P3HT:PCBM film can be reduced from 18.9 nm (ITO/P3HT:PCBM, Figure 3d) to 13.4 nm (ITO/CuO_x/P3HT:PCBM, Figure 3e). Similarly, the rms roughness of the P3HT:ICBA active layer can be reduced from 12.1 nm (ITO/P3HT:ICBA, Figure 3f) to 8.9 nm (ITO/CuO_x/P3HT:ICBA, Figure 3g). The results show that the photoactive layers based on P3HT system show higher roughness than the substrate, regardless of the existence of CuO_x buffer layer modification on the ITO substrate. The increased roughness is the result of phase segregation of P3HT and fullerene derivatives, which facilitates the formation of separate pathways for holes and electrons, respectively.[43] PBDTTT-C:$PC_{70}BM$ film on ITO/CuO_x shows a rms roughness of 1.73 nm (Figure 3i), which is similar to that (1.7 nm) of PBDTTT-C:$PC_{70}BM$ on bare ITO substrate (Figure 3h). It is can be seen that the CuO_x buffer layer has almost no effect on the morphology of the PBDTTT-C:$PC_{70}BM$ film, which could be attributed to the good film forming property of PBDTTT-C.

Panels a and b in Figure 4 shows the device structure and the energy levels of the materials utilized in the devices. The highest occupied molecular orbital (HOMO) and the lowest unoccupied molecular orbital (LUMO) levels for CuO_x are determined to be 5.85 and 3.83 eV by CV (see Figure S2 in the Supporting Information), respectively. The LUMO and HOMO levels of P3HT,[44] PBDTTT-C,[34] PCBM,[45] $PC_{70}BM$,[45] and ICBA[35] are taken from the literature.

Excitons can be formed when photons are absorbed by the photoactive layer. The generated excitons transport to the donor/acceptor interface through diffusion, and dissociate into holes and electrons. The current–voltage characteristics of ITO/CuO_x/Au indicate that the CuO_x forms an ohmic contact with ITO (see Figure S3 in the Supporting Information). The ohmic contact is conducive to the hole extraction at the interface between anode and the photoactive layer, and is able to produce a high built-in electric field, which also benefits to the transportation of the separated charge carriers. Furthermore, the ohmic contact leads to the increase in open-circuit voltage (V_{oc}) by decreasing the contact resistance.[46] Meanwhile, the electrons can be collected by the cathode through the LUMO level of the fullerene acceptor. Therefore, high charge collection efficiency could be achieved from the view of energy level alignment.

The current density–voltage (J–V) curves of the devices in dark and under the illumination of AM 1.5G, 100 mW/cm^2 are shown in Figure 5a–c, and the device parameters are summarized in Table 1. For P3HT:PCBM based devices, reference device A shows a PCE of 2.8%, a short-circuit current density (J_{sc}) of 8.75 mA/cm^2, an open-circuit voltage (V_{oc}) of 0.57 V, and a fill factor (FF) of 56.2%. Upon introduction of PEDOT:PSS buffer layer, the four parameters, PCE, V_{oc}, J_{sc}, and FF, of device B are all enhanced to 3.7%, 0.59 V, 9.11 mA/cm^2, and 68.9%, respectively. The V_{oc} and J_{sc} for device C, which utilized CuO_x as anode buffer layer, can be increased to 0.62 V, 10.81 mA/cm^2, therefore, the maximum PCE can be further enhanced to 4.1% (with an average PCE of 3.97 ±

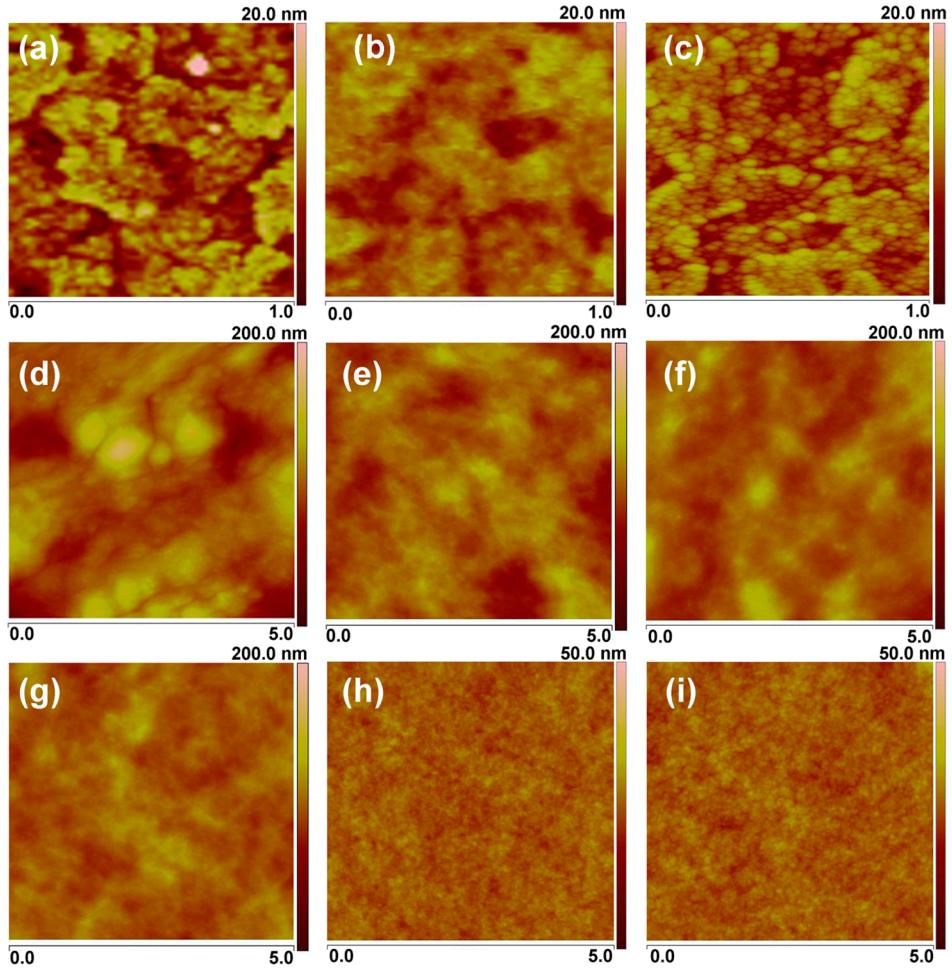

Figure 3. AFM images of (a) bare ITO substrate, (b) PEDOT:PSS on ITO substrate and (c) CuO_x on ITO substrate, with 1 μm × 1 μm scan size. AFM images of (d, e) P3HT:PCBM, (f, g) P3HT:ICBA, and (h, i) PBDTTT-C:$PC_{70}BM$ on ITO and ITO/CuO_x substrate, respectively, with 5 μm × 5 μm scan size.

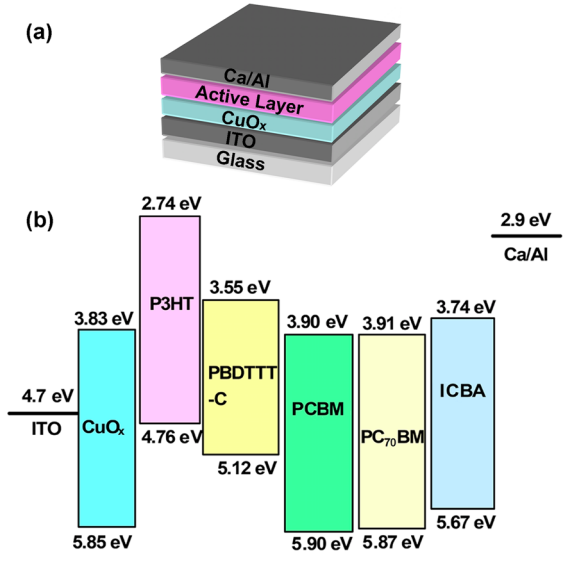

Figure 4. (a) Device structure of the polymer solar cells. (b) The HOMO and LUMO energy levels of the materials involved in the PSCs.

0.04%), which is 46% higher than that of the device A without buffer layer, and 11% higher than that of the device B using PEDOT:PSS hole collection layer. Both J_{sc} and V_{oc} are increased for device C, while the FF is slightly decreased. Series resistance (R_s) and parallel resistance (R_p) for the devices are calculated from the $J-V$ characteristics under dark condition at 0 and 1 V, respectively (summarized in Table 1). The results demonstrate that the insertion of CuO_x layer is able to increase the R_p of the device greatly, and decrease the R_s of the device. The increased J_{sc} of the device C could result from the enhanced hole collection at the CuO_x/P3HT interface by decreasing series resistance from 7.9 Ω cm^2 (device A without buffer layer), to 2.1 Ω cm^2 (device C with CuO_x buffer layer). The decreased R_s for device C may originate from following contributions: more uniform interfacial contact between the photoactive layer and anode because of the smoother surface of CuO_x and high work function of copper oxide (approximately 5.3 eV),[47,48] which benefits the hole collection at the anode/active layer. For organic bulk heterojunction solar cells with ohmic contacts, V_{oc} is controlled by the difference between the LUMO of the acceptor and the HOMO of the donor; it can be expressed by an empirical equation:[49] $V_{oc} = 1/q(|E_{HOMO,D}| - |E_{LUMO,A}|) - 0.3V$. The acceptor and donor materials are same for device A-C. Therefore, the increased V_{oc} of device C with a CuO_x buffer layer, in comparison with the reference devices A and B, could result from the increase in R_p. The insertion of p-type

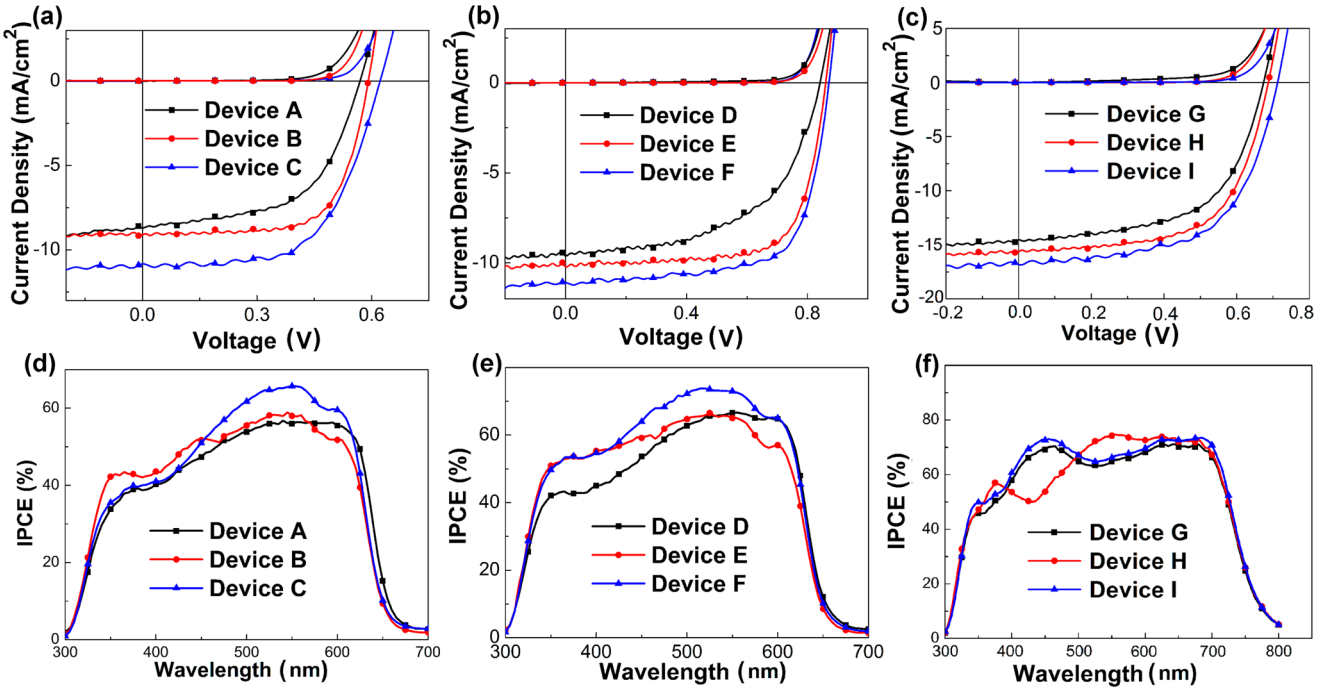

Figure 5. *J*–*V* curves of the PSCs based on (a) P3HT:PCBM, (b) P3HT:ICBA, and (c) PBDTTT-C:$PC_{70}BM$ under the illumination of AM 1.5G, 100 mW/cm^2. Input photon to converted current efficiency (IPCE) spectra of the PSCs based on (d) P3HT:PCBM, (e) P3HT:ICBA, and (f) PBDTTT-C:$PC_{70}BM$.

Table 1. Device Parameters of the PSCs with Different Buffer Layer in the Dark and under the Illumination of AM1.5G, 100 mW/cm^2

				PCE (%)			
devices	V_{oc} (V)	J_{sc} (mA/cm^2)	FF (%)	best	average[a]	R_s[b] (Ω cm^2)	R_p[b] (KΩ cm^2)
A	0.57	8.75	56.2	2.80	2.65 ± 0.04	7.7	62.7
B	0.59	9.11	68.9	3.70	3.58 ± 0.03	3.5	108.8
C	0.62	10.81	61.2	4.10	3.97 ± 0.04	2.1	250.9
D	0.84	9.66	55.4	4.49	4.33 ± 0.04	5.3	71.8
E	0.86	10.27	71.3	6.29	6.05 ± 0.05	3.0	120.8
F	0.87	11.08	69.7	6.72	6.53 ± 0.04	2.2	232.5
G	0.67	14.56	59.8	5.83	5.61 ± 0.04	4.7	92.7
H	0.69	15.67	62.0	6.70	6.49 ± 0.04	2.6	185.4
I	0.71	16.86	59.7	7.14	6.92 ± 0.05	2.3	209.4

[a]The parameters of PCEs were averaged over ten devices. [b]Parallel resistance (R_p) and series resistance (R_s) for PSCs in the dark are obtained at around 0 and 1 V, respectively.

semiconductor copper oxide reduces separated charge recombination through improving hole selectivity at the CuO_x/photoactive layer heterointerface.

ICBA is a kind of C_{60} derivative that shows better absorption properties in the visible range and solubility in commonly used organic solvents. ICBA possesses a higher LUMO (0.17 eV) level than PCBM, therefore, PSCs with P3HT:ICBA as photoactive layer could show higher V_{oc} than P3HT:PCBM based PSCs.[35] As for the PSCs with ICBA as the acceptor, the four parameters for device D without buffer layer, PCE, V_{oc}, J_{sc}, and FF are 4.49%, 0.84 V, 9.66 mA/cm^2, and 55.4%, respectively. Device E with PEDOT:PSS buffer layer exhibits a higher PCE of 6.29%. By contrast, even higher PCE of 6.72% (with an average value of 6.53 ± 0.04%) can be realized by using CuO_x as buffer layer (device F), which is 50% higher than that of the device D without buffer layer.

To verify the compatibility of CuO_x layer with different electron donor materials and further improve the efficiency of the device, a representative low-band-gap D–A copolymer, PBDTTT-C, is selected as donor material for device G-I. The PBDTTT-C based devices exhibit much higher J_{sc} than P3HT based devices due to the broad absorption of PBDTTT-C. For reference device G without buffer layer, it shows a PCE of 5.83%, a V_{oc} of 0.67 V, a J_{sc} of 14.56 mA/cm^2, and an FF of 59.8%. Device H adopted PEDOT:PSS as hole collection layer exhibits an enhanced PCE of 6.7%, a J_{sc} of 15.67 mA/cm^2 and a V_{oc} of 0.69 V. For device I with CuO_x buffer layer, the PCE was further enhanced to 7.14% (with an average value of 6.92 ± 0.05%), with an increased J_{sc} of 16.86 mA/cm^2 and a V_{oc} of 0.71 V.

To clarify the enhanced J_{sc} for CuO_x modified devices, we compared the IPCE spectra of the PSCs A–I (Figure 5d–f). For P3HT:PCBM-based or P3HT:ICBA-based devices, the IPCE spectra show similar characteristics, respectively. For devices B and E with PEDOT:PSS buffer layer, the IPCE spectra show slightly higher light response in the range of 350–

500 nm, which results from higher transparency of ITO/PEDOT:PSS substrate in this wavelength range, as shown in Figure S1 in the Supporting Information. The devices with CuO_x buffer layer show higher IPCE, which is consistent with the higher J_{sc} of the corresponding PSCs. The IPCE spectra of PBDTTT-C based devices without buffer layer (device G) and with CuO_x buffer layer (device I) show similar characteristics, however, device H with PEDOT:PSS buffer layer shows totally different light response in the wavelength range of 400−600 nm. There exists a deep valley for PEDOT:PSS-modified device in the wavelength range of 400−500 nm, which is consistent with the results reported in previous literature.[6] Further investigation is in progress to provide better understanding of this phenomenon.

The AC impedance spectroscopy was performed to investigate the change in interface resistance of the PSCs upon introduction of CuO_x layer. The impedance measurements were performed with a CHI650D Electrochemical Workstation with an 20 mV ac signal at frequencies from 1 MHz to 1 Hz, under the illumination of AM 1.5G, 100 mW/cm^2. A bias voltage equal to V_{oc} was applied to vanish the total current. The Nyquist plots of the AC impedance of P3HT:PCBM based devices A-C are demonstrated in Figure 6. Figure 6a shows the equivalent modeled circuit.[50] which

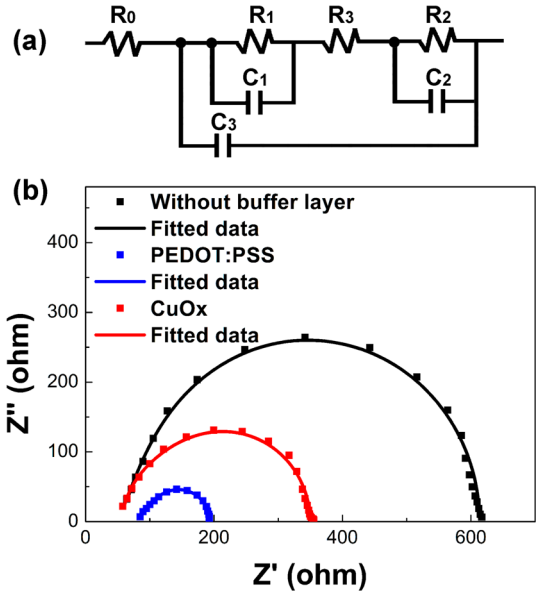

Figure 6. (a) Equivalent modeled circuits of the PSCs. (b) Nyquist plot of the devices based on P3HT:PCBM under the illumination of AM 1.5G, 100 mW/cm^2 at a bias equal to V_{oc}, the inset is the equivalent modeled circuit.

comprises a serial resistance (R_0) and three RC networks. The serial resistance (R_0) is mainly ascribed to the ITO contact. The RC networks comprise a capacitance (C_3) paralleled to a serial network, which contains R_1 parallel to capacitance (C_1), R_2 parallel to C_2, and R_3. The RC elements, R_1/C_1, R_2/C_2, and R_3/C_3, are assigned to the depletion layer between the photoactive and the metal cathode, anode buffer layer and photoactive layer, respectively. The equivalent circuit omitted RC element R_2/C_2 is used to fit the experimental data for device A without a buffer layer. The fitted data of the impedance spectroscopy analysis indicate that R_0 is 61, 58, and 85 Ω for devices A, B, and C, respectively, which means that the serial resistance at the ITO anode is slightly increased upon modification of CuO_x buffer layer. However, R_3, the resistance corresponding to the photoactive layer, shows a large decrease upon variation of anode modification layers. R_3 is 217, 188, and 58 Ω for devices A, B, and C, respectively. R_2, which is assigned to the anode buffer layer, also decreases from 103 to 48 Ω when using CuO_x instead of PEDOT:PSS as anode buffer layer. The decreased R_2 and R_3 upon modification of CuO_x layer could be the reason for the increased device performance.

4. CONCLUSIONS

In conclusion, highly efficient polymer solar cells have been achieved by introducing solution processed nontoxic CuO_x as anode buffer layer. The CuO_x layer can be easily obtained from a 1,2-dichlorobenzene solution of $Cu(acac)_2$ precursor with thermal annealing at lower temperature (80 °C) in air. The CuO_x layer shows high light transmittance. The high work function of CuO_x enables it to effectively extract holes. An ohmic contact can be formed and the resistance of the whole device can be decreased through the introduction of CuO_x layer, which enhances PCE of the device by reducing the separated charge recombination losses. The PSCs with the CuO_x buffer layer exhibits enhanced performance than the PEDOT:PSS-based PSCs, and the PCE of the PSCs using narrow bandgap conjugated polymer (PBDTTT-C) as donor material can reach as high as 7.14%.

■ ASSOCIATED CONTENT

Supporting Information

Optical transmittance spectra of the PEDOT:PSS and the CuO_x interfacial layer on ITO coated glass; Cyclic voltammograms of the CuO_x film on platinum electrode after thermal annealing in air at 80 °C for 20 min. This material is available free of charge via the Internet at http://pubs.acs.org.

■ AUTHOR INFORMATION

Corresponding Authors

*E-mail: tanzhanao@ncepu.edu.cn (Z.A.T.).
*E-mail: liyf@iccas.ac.cn (Y.F.L.).

Author Contributions

Authors Q.X. and F.W. contributed equally to this work.

Notes

The authors declare no competing financial interest.

■ ACKNOWLEDGMENTS

The work was supported by the NSFC (21004019, 51173040, 51303052), the Ministry of Science and Technology of China (863 project, 2011AA050523), the Beijing NOVA Program (2010B038), SRFDP (20100036120007), Program for New Century Excellent Talents in University (NCET-12-0848), and Fundamental Research Funds for the Central Universities, China (11QG18, 13ZD11).

■ REFERENCES

(1) Service, R. F. *Science* **2011**, *332*, 293.
(2) Günes, S.; Neugebauer, H.; Sariciftci, N. S. *Chem. Rev.* **2007**, *107*, 1324−1338.
(3) Li, Y. F. *Acc. Chem. Res.* **2012**, *45*, 723−733.
(4) Gaudiana, R.; Brabec, C. *Nat. Photonics* **2008**, *2*, 287−289.
(5) Tan, Z. A.; Zhang, W. Q.; Zhang, Z.; Qian, D. P.; Huang, Y.; HOU, J.; Li, Y. F. *Adv. Mater.* **2012**, *24*, 1476−1481.
(6) Huo, L. J.; Zhang, S. Q.; Guo, X.; Xu, F.; Li, Y. F.; Hou, J. H. *Angew. Chem., Int. Ed.* **2011**, *50*, 9697−9702.

(7) Meng, X.; Zhang, W.; Tan, Z. A.; Li, Y. F.; Ma, Y.; Wang, T.; L., J.; Shu, C.; Wang, C. *Adv. Funct. Mater.* **2012**, *22*, 2187−2193.
(8) Girotto, C.; Voroshazi, E.; Cheyns, D.; Heremans, P.; Rand, B. P. *ACS Appl. Mater. Interfaces* **2011**, *3*, 3244−3247.
(9) He, Z. C.; Zhong, C. M.; Su, S. J.; Xu, M.; Wu, H. B.; Cao, Y. *Nat. Photonics* **2012**, *6*, 593−597.
(10) You, J. B.; Dou, L. T.; Yoshimura, K.; Kato, T.; Ohya, K.; Moriarty, T.; Emery, K.; Chen, C.-C.; Gao, J.; Li, G.; Yang, Y. *Nat. Commun.* **2013**, *4*, 1446.
(11) Brown, T. M.; Kim, J. S.; Friend, R. H.; Cacialli, F.; Daik, R.; Feast, W. J. *Appl. Phys. Lett.* **1999**, *75*, 1679−1681.
(12) Kirchmeyer, S.; Reuter, K. *J. Mater. Chem.* **2005**, *15*, 2077−2088.
(13) Norrman, K.; Madsen, M. V.; Gevorgyan, S. A.; Krebs, F. C. *J. Am. Chem. Soc.* **2010**, *132*, 16883−16892.
(14) Nardes, A. M.; Kemerink, M.; de Kok, M. M.; Vinken, E.; Maturova, K.; Janssen, R. A. J. *Org. Electron.* **2008**, *9*, 727−734.
(15) Norrman, K.; Gevorgyan, S. A.; Krebs, F. C. *ACS Appl. Mater. Interfaces* **2009**, *1*, 102−112.
(16) Dang, X. D.; Dante, M.; Nguyen, T. Q. *Appl. Phys. Lett.* **2008**, *93*, 241911.
(17) Tan, Z. A.; Qian, D. P.; Zhan, X. W.; Li, L. J.; Ding, Y. Q.; Xu, Q.; Wang, F. Z.; Li, Y. F. *J. Mater. Chem. A* **2013**, *1*, 657−664.
(18) Tan, Z. A.; Zhang, W. Q.; Cui, C. H.; Ding, Y. Q.; Qian, D. P.; Xu, Q.; Li, L. J.; Li, S. S.; Li, Y. F. *Phys. Chem. Chem. Phys.* **2012**, *14*, 14589−14595.
(19) Tan, Z. A.; Li, L. J.; Cui, C. H.; Ding, Y. Q.; Xu, Q.; Li, S. S.; Qian, D. P.; Li, Y. F. *J. Phys. Chem. C* **2012**, *116*, 18626−18632.
(20) Zilberberg, K.; Gharbi, H.; Behrendt, A.; Trost, S.; Riedl, T. *ACS Appl. Mater. Interfaces* **2012**, *4*, 1164−1168.
(21) Zilberberg, K.; Trost, S.; Schmidt, H.; Riedl, T. *Adv. Energy Mater.* **2011**, *1*, 377−381.
(22) Steirer, K. X.; Ndione, P. F.; Widjonarko, N. E.; Lloyd, M. T.; Meyer, J.; Ratcliff, E. L.; Kahn, A.; Armstrong, N. R.; Curtis, C. J.; Ginley, D. S.; Berry, J. J.; Olson, D. C. *Adv. Energy Mater.* **2011**, *1*, 813−820.
(23) Choi, H.; Kim, B.; Ko, M. J.; Lee, D.-K.; Kim, H.; Kim, S. H.; Kim, K. *Org. Electron.* **2012**, *13*, 959−968.
(24) Wu, D.; Zhang, Q.; Tao, M. *Phys. Rev. B* **2006**, *73*, 235206.
(25) Hoa, N. D.; An, S. Y.; Dung, N. Q.; Van Quy, N.; Kim, D. *Sens. Actuators, B* **2010**, *146*, 239−244.
(26) Yang, W.-Y.; Rhee, S.-W. *Appl. Phys. Lett.* **2007**, *91*, 232907.
(27) Musselman, K. P.; Marin, A.; Wisnet, A.; Scheu, C.; MacManus-Driscoll, J. L.; Schmidt-Mende, L. *Adv. Funct. Mater.* **2011**, *21*, 573−582.
(28) Hameş, Y.; Eren San, S. *Sol. Energy* **2004**, *77*, 291−294.
(29) Marin, A. T.; Muñoz-Rojas, D.; Iza, D. C.; Gershon, T.; Musselman, K. P.; MacManus-Driscoll, J. L. *Adv. Funct. Mater.* **2013**, *23*, 3413−3419.
(30) Kidowaki, H.; Oku, T.; Akiyama, T.; Suzuki, A.; Jeyadevan, B.; Cuya, J. *J. Mater. Sci. Res.* **2012**, *1*, 138−143.
(31) Mittiga, A.; Salza, E.; Sarto, F.; Tucci, M.; Vasanthi, R. *Appl. Phys. Lett.* **2006**, *88*, 163502.
(32) Lin, M.-Y.; Lee, C.-Y.; Shiu, S.-C.; Wang, I.-J.; Sun, J.-Y.; Wu, W.-H.; Lin, Y.-H.; Huang, J.-S.; Lin, C.-F. *Org. Electron.* **2010**, *11*, 1828−1834.
(33) Jayatissa, A. H.; Guo, K.; Jayasuriya, A. C. *Appl. Surf. Sci.* **2009**, *255*, 9474−9479.
(34) Hou, J. H.; Chen, H. Y.; Zhang, S. Q.; Chen, R. I.; Yang, Y.; Wu, Y.; Li, G. *J. Am. Chem. Soc.* **2009**, *131*, 15586−15587.
(35) He, Y. J.; Chen, H. Y.; Hou, J. H.; Li, Y. F. *J. Am. Chem. Soc.* **2010**, *132*, 1377−1382.
(36) Okada, K.; Kawai, J.; Kotani, A. *Phys. Rev. B* **1993**, *48*, 10733−10738.
(37) Klein, J. C.; Li, C. P.; Hercules, D. M.; Black, J. F. *Appl. Spectrosc.* **1984**, *38*, 729−734.
(38) Ghijsen, J.; Tjeng, L. H.; van Elp, J.; Eskes, H.; Westerink, J.; Sawatzky, G. A.; Czyzyk, M. T. *Phys. Rev. B* **1988**, *38*, 11322−11330.
(39) Chusuei, C. C.; Brookshier, M. A.; Goodman, D. W. *Langmuir* **1999**, *15*, 2806−2808.
(40) Yin, M.; Wu, C.-K.; Lou, Y.; Burda, C.; Koberstein, J. T.; Zhu, Y.; O'Brien, S. *J. Am. Chem. Soc.* **2005**, *127*, 9506−9511.
(41) Choi, G.-W.; Lee, K.-Y.; Kim, N.-H.; Park, J.-S.; Seo, Y.-J.; Lee, W.-S. *Microelectron. Eng.* **2006**, *83*, 2213−2217.
(42) Sun, Y. M.; Seo, J. H.; Takacs, C. J.; Seifter, J.; Heeger, A. J. *Adv. Mater.* **2011**, *23*, 1679−1683.
(43) Li, G.; Shrotriya, V.; Huang, J. S.; Yao, Y.; Moriarty, T.; Emery, K.; Yang, Y. *Nat. Mater.* **2005**, *4*, 864−868.
(44) Hou, J. H.; Tan, Z. A.; Yan, Y.; He, Y. J.; Yang, C. H.; Li, Y. F. *J. Am. Chem. Soc.* **2006**, *128*, 4911−4916.
(45) He, Y. J.; Zhao, G. J.; Peng, B.; Li, Y. F. *Adv. Funct. Mater.* **2010**, *20*, 3383−3389.
(46) Meyer, J.; Kröger, M.; Hamwi, S.; Gnam, F.; Riedl, T.; Kowalsky, W.; Kahn, A. *Appl. Phys. Lett.* **2010**, *96*, 193302.
(47) Murdoch, G.; Greiner, M.; Helander, M.; Wang, Z.; Lu, Z. *Appl. Phys. Lett.* **2008**, *93*, 083309.
(48) Liu, Y.; Liao, L.; Li, J.; Pan, C. *J. Phys. Chem. C* **2007**, *111*, 5050−5056.
(49) Scharber, M. C.; Mühlbacher, D.; Koppe, M.; Denk, P.; Waldauf, C.; Heeger, A. J.; Brabec, C. J. *Adv. Mater.* **2006**, *18*, 789−794.
(50) Knipper, M.; Parisi, J.; Coakley, K.; Waldauf, C.; Brabec, C. J.; Dyakonov, V. *Z. Naturforsch., A* **2007**, *62a*, 490−494.